Atomic-scale investigation of precipitate phases in QE22 Mg alloy

Xiaojun Zhao[a], Zhiqiao Li[b], Aiping Zhang[b], Longlong Hao[b], Houwen Chen[b]*, Jian-Feng Nie[c]*

[a] Key Laboratory of Advanced Technologies of Materials, Ministry of Education, Southwest Jiaotong University, Chengdu, Sichuan 610031, P.R. China
[b] International Joint Laboratory for Light Alloys (MOE), College of Materials Science and Engineering, Chongqing University, Chongqing 400044, P.R. China
[c] Department of Materials Science and Engineering, Monash University, Victoria 3800, Australia

*Corresponding authors

E-mail addresses: hwchen@cqu.edu.cn (H.W. Chen), and jianfeng.nie@monash.edu (J.F. Nie)

Abstract

Precipitation-hardenable commercial Mg alloy QE22 (Mg-2.5Ag-2.0Nd-0.7Zr, wt.%) has excellent mechanical properties, but precipitates in this alloy have not been well understood. In this work, precipitate phases γ", γ and δ formed during isothermal ageing process at 150 ºC, 200 ºC, 250 ºC and 300 ºC have been characterized using atomic-resolution high-angle annular dark-field scanning transmission electron microscopy and atomic-scale energy-dispersive X-ray spectroscopy. The morphology, crystal structure and orientation relationship of these precipitate phases have been determined. Domain boundaries usually exist in a single γ particle, which can be characterized by a separation vector of $[1\bar{1}01]_{\alpha}$. The δ phase forms *in situ* from its precursor γ phase, consequently leading to the formation of three different variants within a single δ particle. The nucleation of δ phase is strongly related to the domain boundaries of the γ phase. The formation of the γ phase may be promoted by its precursor γ" phase. The similarities in atomic structures of the γ", γ and δ phases are described and discussed, indicating that transformations between these precipitate phases can be accomplished through the diffusion of added alloying elements.

Keywords: Magnesium alloy; Precipitation; Phase identification; Phase transformation; Electron microscopy

1. Introduction

Mg alloys have received much attention in the past two decades due to their light weight and high specific strength [1-4]. An important alloy group include Mg-RE (rare earth) based alloys, which have the potential to develop alloys with high strength and excellent creep resistance [5-10]. Mg-RE alloys exhibit a moderate age hardening response, and most Mg-RE alloys such as Mg-Gd, Mg-Nd, Mg-Gd-Y, and Mg-Y-Nd have a similar precipitation sequence, including the formation of β-type precipitates such as β'', β', β_1 and β [11-17]. The β-type precipitates usually form as plates with habit planes lying parallel to prismatic planes of the α-Mg lattice, i.e. $\{10\bar{1}0\}_\alpha$ or $\{11\bar{2}0\}_\alpha$ planes. Additions of Ag to many Mg-RE alloys can considerably enhance the age hardening response and ultimately improve the yield strength of these alloys, such as Mg-Y-Zn-Ag, Mg-Gd-Ag and Mg-Gd-Y-Ag alloys [18-25]. With the addition of Ag, another Mg-RE-Ag ternary γ-type precipitates, which usually form as plates with their habit plane lying parallel to the $(0001)_\alpha$ basal plane of α-Mg, appear solely or together with β-type precipitates in these alloys.

The addition of Ag to Mg-Nd alloys has led to the development of a commercial Mg alloy QE22 (Mg-2.5Ag-2Nd-0.7Zr, wt.%) [26]. QE22 is well known for its good tensile properties at elevated temperature and creep resistance and has been used in the aircraft and aerospace industries [5, 8]. However, the precipitate phases involved in the ageing process of QE22 have not been well understood, particularly at atomic scale [5]. Two metastable phases, β and γ, and an equilibrium phase were initially reported [27]. β reportedly has a hexagonal structure (a = 0.556 nm, c = 0.521 nm), and its orientation relationship with respect to α-Mg is such that $(0001)_\beta$ // $(0001)_\alpha$ and $[01\bar{1}0]_\beta$ // $[2\bar{1}\bar{1}0]_\alpha$. γ has also been reported to have a hexagonal structure (a = 0.963 nm, c = 1.024 nm), but the orientation relationship between γ and α-Mg was not mentioned in that work. A more recent work also reported the presence of two metastable hexagonal phases χ and γ, based on selected area electron diffraction (SAED) patterns [28]. The χ phase has lattice parameters of a = 0.286 nm, c = 0.521 nm, and the orientation relationship between χ and α-Mg is identical to that between β and α-Mg. The crystal structure of the γ phase was reported to be the same as that of γ phase in a previous work [27], and the orientation relationship between γ and α-Mg is such that $(0001)_\gamma$ // $(0001)_\alpha$ and $[2\bar{1}\bar{1}0]_\gamma$ // $[2\bar{1}\bar{1}0]_\alpha$ [28]. The crystal structure of the equilibrium phase is controversial in previous reports [27-29]. In our recent work, we carefully studied the equilibrium intermetallic phase formed in grain boundaries of QE22 alloy, by using modern techniques such as atomic-resolution high-angle annular dark-field scanning transmission electron microscopy (HAADF-STEM) and energy-dispersive X-ray spectroscopy (EDXS). This equilibrium phase (designated δ) was determined to have an orthorhombic structure (space group *Cmcm*, a = 1.02 nm, b = 1.18 nm, c = 1.00 nm) with a stoichiometry of $NdAgMg_{11}$ [30]. However, the precipitation behavior of the equilibrium δ phase during ageing process is still unclear. Therefore, controversies and uncertainties remain on both metastable and equilibrium phases, and their precipitation during ageing, in QE22 alloy.

The purpose of the present work is to systematically study the morphology, crystal structure, orientation relationship of these precipitate phases as well as the underlying evolution process among these phases. Two metastable phases γ'' and γ, and an equilibrium phase δ are characterized in detail at atomic level. The crystal structure of the γ phase is proposed and validated by density functional theory (DFT) calculation and image simulation. The domain boundaries inside the γ phase are observed, and their influence on the *in situ* formation of δ phase is discussed. This work provides an in-depth understanding of precipitate phases and precipitation processes in Mg-RE-Ag alloys.

2. Material and methods

As-cast commercial QE22 alloy bars with a nominal composition of Mg-2.5Ag-2.0Nd-0.7Zr (wt.%) were used. The actual composition was measured by inductively coupled plasma atomic emission spectroscopy to be Mg-3.01Ag-2.10Nd-0.34Zr (wt.%). Bulk samples with dimensions of 10 mm × 10 mm × 10 mm were covered with MgO powder, solution treated in a muffle furnace at 520 ºC for 6 h and then water quenched at ambient temperature. Ageing treatment was then conducted in oil baths at 150 ºC, 200 ºC, 250 ºC and 300 ºC, respectively. Samples for transmission electron microscopy (TEM) were cut into 500 μm thick slices from the bulk samples. These slices were polished to 50-70 μm thick, punched to discs with 3 mm in diameter, and then ion-beam milled using Gatan PIPS 691 at -70 ºC. HAADF-STEM images and atomic-scale EDXS-STEM maps were acquired from a Cs-corrected FEI Titan G^2 60-300 ChemiSTEM, which equipped with a high-brightness X-FEG electron source and a Super-X EDXS detector consisting of 4 windowless silicon-drift detectors. Accelerating voltages for HAADF-STEM and EDXS-STEM were 300 kV and 120 kV, respectively. A convergence semi-angle of 15 mrad and collection semi-angle of 45-262 mrad were used. The acquisition time for each EDXS data is approximately within the range of 100 to 150 seconds. HAADF-STEM image simulations were performed using xHREM software. The atomic-resolution HAADF-STEM images were Fourier filtered and the atomic-scale EDXS maps were Wiener filtered using Gatan DigitalMicrograph software.

Theoretical simulations based on DFT were completed using Vienna Ab initio Simulation Package (VASP) code [31]. The generalized gradient approximation of Perdew-Burke-Ernzerhof (GGA-PBE) [32] was utilized in handling electron exchange and correlation. For pseudopotential selection, the valence electron configurations of element Mg, Ag and Zn were described using the settings recommended by VASP. For the aim of obtaining the precise crystal structure and thermodynamical stability of the precipitate phase, the *f*-electrons of rare-earth element Gd and Nd were treated to be included in pseudo-core, which gives efficient calculation performance and accurate results [30, 33-35]. The energy and force convergence criteria were set to be 10^{-6} eV and 10^{-2} eV/Å, respectively. Series of cut-off energy values were tested, and the value was finally chosen to be 400 eV. The formation energy (E_f) is calculated to be the difference per atom between the total energy of input supercell and the sum of chemical potentials of every atom, the equation:

$$E_f = (E_{tot} - \Sigma n_i \mu_i) / \Sigma n_i, \quad (1)$$

where E_{tot} is the total energy of the input supercell, $\Sigma n_i \mu_i$ is the sum of chemical potentials of all contained atoms and Σn_i is the number of atoms in the supercell. Here, the chemical potential μ of each element is calculated using their bulk materials.

3. Results

3.1 Metastable γ'' and γ precipitate phases

Two metastable precipitate phases formed in samples aged at 200 ºC and 150 ºC are firstly investigated. Ageing for approximately 10 hours at 200 ºC has been widely accepted as the peak-aged condition (T6 treatment) of QE22 alloy [5, 28]. The microstructure of a sample aged for 1 hour at 200 ºC, i.e. under-aged condition, is provided in Figs. 1a and 1c, which are viewed along $[2\bar{1}\bar{1}0]_\alpha$ and $[0001]_\alpha$ of α-Mg matrix, respectively. The dominant precipitates at this ageing stage are densely distributed plate-like precipitates with their habit plane lying parallel to the $(0001)_\alpha$ basal plane, as indicated by green arrows in Figs. 1a and 1c. In addition to the basal plates, sparsely distributed diamond-shaped particles could also be observed, as shown by yellow arrows in Figs. 1a and 1c. The

basal plates and diamond-shaped particles are confirmed to be γ" and γ phase respectively, based on subsequent atomic-resolution investigations. In such under-aged condition, the γ" phase is typically about 6 nm in diameter and 0.45 nm in thickness, and thus its aspect ratio is approximately 13.3, while the size of γ phase is about 6 nm. Since the γ" phase is very thin, its contrast in a HAADF-STEM image viewed along the $[0001]_\alpha$ direction is much weaker than that of the γ phase, as shown in Fig. 1c. With continued ageing to 10 hours at 200 ºC, i.e. peak-aged condition, the precipitates observed are only γ particles, while the γ" plates have disappeared, as shown in Figs. 1b and 1d. The γ particles have a size of about 10 nm in such peak-aged condition. Similar precipitation behavior is also observed during ageing at 150 ºC. Typical microstructures of samples aged for 16 hours and 120 hours are shown in Figs. 1e and 1f, which illustrates that the dominate precipitate phase in the two ageing stages is γ" and γ phase, respectively. Since HAADF-STEM images are Z-contrast, the brighter contrast of both γ" and γ indicates that they contain heavy elements Nd, Ag or both. EDXS mapping is performed on the two types of precipitates to figure out their chemical information, as shown in Fig. 2, which clearly shows that they contain both Nd and Ag elements.

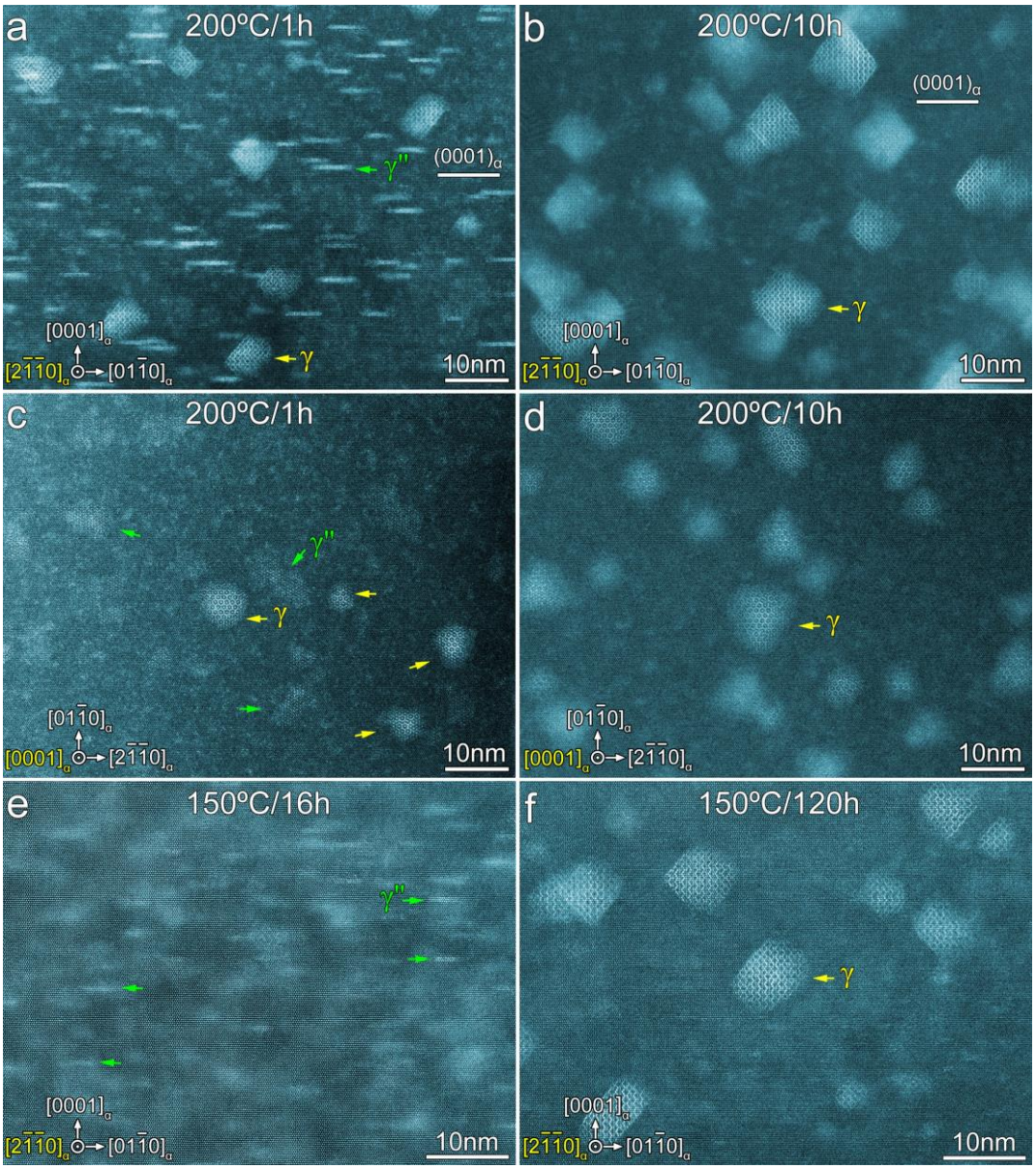

Fig. 1 Low-magnification HAADF-STEM images showing the morphology and distribution of metastable precipitate phases γ" and γ in samples with different ageing conditions as noted. Electron

beam is parallel to $[2\bar{1}\bar{1}0]_\alpha$ in (a, b, e, f), and $[0001]_\alpha$ in (c, d).

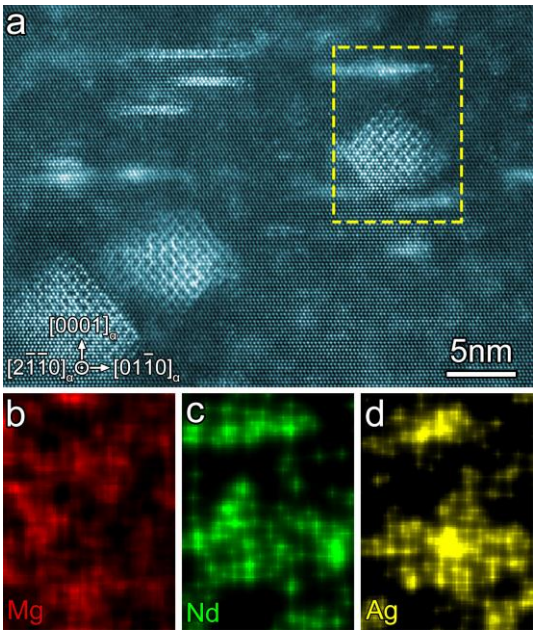

Fig. 2 (a) HAADF-STEM image showing the γ" plates and γ particles in a sample aged for 1 hour at 200 ºC. (b-d) EDXS maps showing the distribution of Mg, Nd and Ag in the region delimited by the yellow dashed rectangle in (a). Electron beam is parallel to $[2\bar{1}\bar{1}0]_\alpha$.

Figs. 3a-3c show the atomic-resolution HAADF-STEM images of the γ" plates viewed along three principal zone axes of α-Mg matrix. The γ" phase is coherent with their surrounding α-Mg matrix. Viewed along the $[2\bar{1}\bar{1}0]_\alpha$ direction, Fig. 3a, the γ" phase contains only three atomic layers. The stacking sequence of the three atomic layers is different from the original ABA-type sequence of α-Mg matrix. The atomic sites in the middle layer locate at the intersection point of the diagonals of the red frame in the inset of Fig. 3a, which is defined as a new position D. The γ" phase thus has an ADA-type stacking sequence. It seems that the bright atomic columns in the outer two layers are elliptical and elongates a little bit along the vertical direction of Fig. 3a, i.e. the $[0001]_\alpha$ direction. The reason for this phenomenon is that the outer two layers are not flat, which can be confirmed when viewed along the $[01\bar{1}0]_\alpha$ direction, as shown in Fig. 3b. The interplanar spacing of the outer two layers measured from Fig. 3a and Fig. 3b is 0.45 nm and 0.41 nm (±0.01 nm) respectively if c = 0.521 nm is assumed for the α-Mg matrix. Viewed along the $[0001]_\alpha$ direction, Fig. 3c, the bright columns occupy the positions of original Mg columns of α-Mg matrix and are arranged in a triangular shape with the interatomic spacing of 0.56 nm (±0.01 nm). Based on the combined analyses of the atomic arrangements in Figs. 3a-3c, the atomic structure of the basal plate is identical to that of the γ" phase reported in Mg-Gd-Ag, Mg-Y-Zn-Ag, and Mg-Gd-Zn alloys [19, 21, 36, 37]. For this reason, such basal plates in the present Mg-Nd-Ag alloy are also designated γ". The γ" phase has a hexagonal structure with lattice parameters of a = 0.56 nm and c = 0.45 nm. The atomic model of γ" has been proposed in the literature and has been extensively studied through DFT calculations [19, 37]. But it is the first time for the γ" phase being observed in QE22 alloy. The orientation relationship between γ" and α-Mg is such that $(0001)_{\gamma''}$ // $(0001)_\alpha$ and $[01\bar{1}0]_{\gamma''}$ // $[2\bar{1}\bar{1}0]_\alpha$.

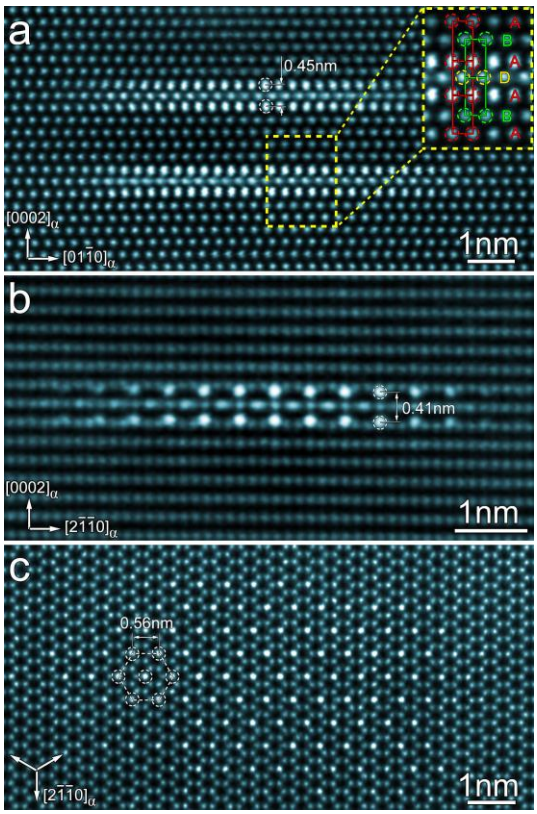

Fig. 3 Atomic-resolution HAADF-STEM images of the γ" basal plates in a sample aged for 1 hour at 200 ºC. Electron beam is parallel to (a) $[2\bar{1}\bar{1}0]_\alpha$, (b) $[01\bar{1}0]_\alpha$ and (c) $[0001]_\alpha$. Inset in (a) is a magnified view of the region enclosed by the yellow dashed rectangle.

Figs. 4a-4c show the atomic-resolution HAADF-STEM images of the γ particles viewed along three principal zone axes of α-Mg matrix in a sample aged for 10 hours at 200 ºC. The γ phase is coherent with its surrounding α-Mg matrix, and misfit dislocations are not found in its interphase boundaries. When the γ particle is viewed along the $[0001]_\alpha$ direction, the characteristic of bright columns arranged in a hexagonal shape can be clearly observed, as indicated by orange hexagons in Fig. 4a. Several domains can be often observed in a single γ particle viewed along the $[0001]_\alpha$ direction. In each domain, the crystallographic orientation of γ phase is the same, but the translation symmetry of the characteristic hexagons between two domains is broken by the domain boundaries (indicated by white dashed lines in Fig. 4a), which are parallel to $<2\bar{1}\bar{1}0>_\alpha$ directions. Viewed along the $[2\bar{1}\bar{1}0]_\alpha$ direction, Fig. 4b, the main characteristic of the γ particle is that the bright columns are arranged in a shape of zig-zag chains. Again, different domains can be usually observed, and the zig-zag chains reverse in adjacent domains. The domain boundaries are indicated by the white dashed lines in Fig. 4b, which are parallel to the $[0001]_\alpha$ direction. However, domain boundaries are not found when viewed along the $[01\bar{1}0]_\alpha$ direction. Details of the domain boundaries in the γ phase will be discussed in section 4.1.

According to the combined analyses of the periodicities of the atomic columns in Figs. 4a-4c, a hexagonal unit cell is determined, whose projections along corresponding zone axes are indicated by green frames in Figs. 4a-4c. The lattice parameters are measured to be a = 0.99 nm, c = 1.03 nm (±0.01 nm), under the assumption of a = 0.321 nm for the α-Mg matrix. Corresponding FFT patterns are also provided in Figs. 4d-4f, which can be indexed based on this hexagonal structure. The lattice parameters measured in this work are similar to those of the γ phase reported in previous studies of QE22 alloy [27, 28], and for this reason such diamond-shaped particle observed in present work is

designated γ. It is the first time that the atomic structure of the γ phase is observed directly. The orientation relationship between γ phase and α-Mg matrix is such that $(0001)_\gamma$ // $(0001)_\alpha$ and $[2\bar{1}\bar{1}0]_\gamma$ // $[2\bar{1}\bar{1}0]_\alpha$.

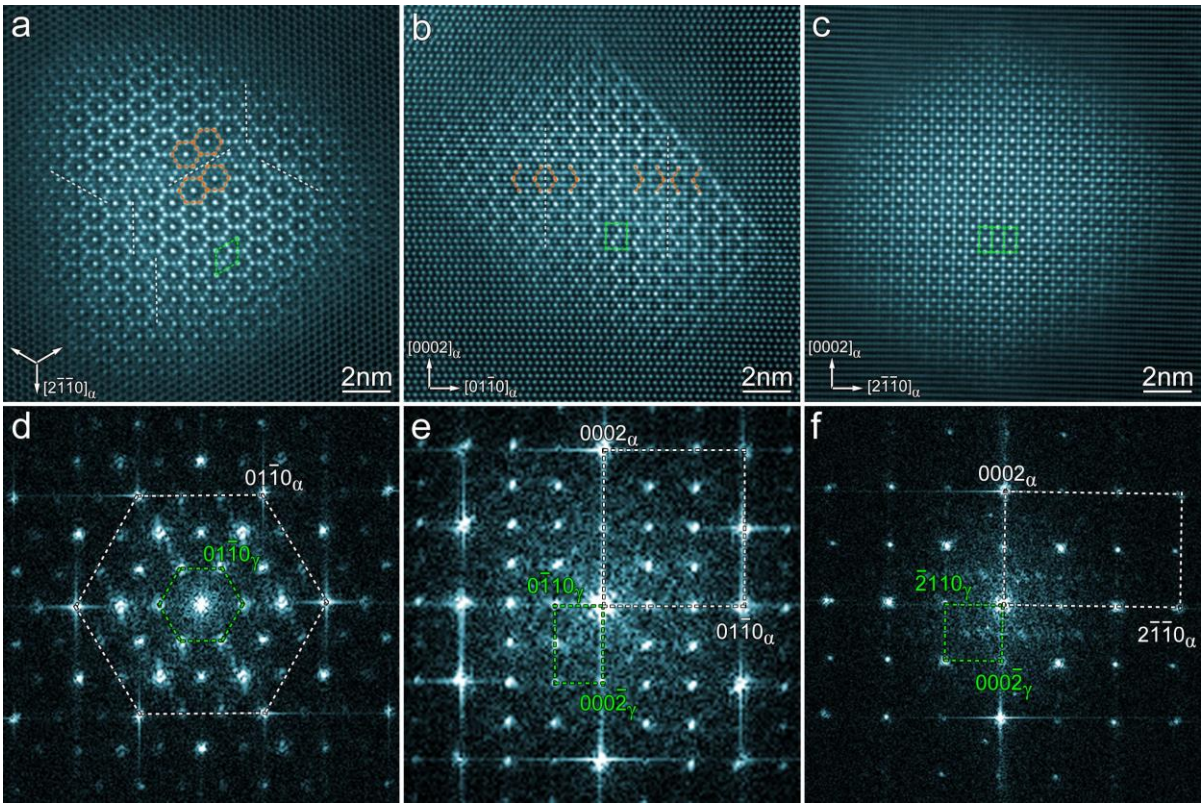

Fig. 4 (a-c) Atomic-resolution HAADF-STEM images of the diamond-shaped γ particles in a sample aged for 10 hours at 200 ºC. Orange dashed lines in (a, b) indicate corresponding characteristics of the atomic arrangements. White dashed lines in (a, b) show positions of domain boundaries. Green dashed lines in (a-c) represent projections of a γ unit cell along corresponding zone axis. (d-e) Corresponding FFT patterns of (a-c). Electron beam is parallel to (a) $[0001]_\alpha$, (b) $[2\bar{1}\bar{1}0]_\alpha$ and (c) $[01\bar{1}0]_\alpha$.

To investigate the atomic structure of the γ phase, combined atomic-resolution HAADF-STEM images and EDXS maps are provided in Fig. 5. Although HAADF-STEM images are Z-contrast, the intensity of individual columns is also related to the packing density of atoms in each column. Ambiguities might remain if the elemental information of a single column is deduced based only on HAADF-STEM images, especially in situations involving multiple alloying elements. In the present study of the Mg-Nd-Ag ternary precipitates, atomic-scale EDXS mapping is performed to precisely distinguish the Nd-rich and Ag-rich columns. Figs. 5a-5c show atomic-resolution HAADF-STEM images of γ particles viewed along three principal zone axes of α-Mg, while Figs. 5d-5l show corresponding EDXS maps. Viewed along the $[0001]_\alpha$ direction, Nd-rich columns can be determined unambiguously by Nd map in Fig. 5d, which locate at the center and six vertexes of each characteristic hexagon, forming a trigonal distribution, as indicated by yellow dashed circles in Figs. 5a and 5d. In Fig. 5g, Ag-rich columns are not well resolved because they are more sensitive to electron beam during the acquisition EDXS data. Nevertheless, Ag-rich columns can be deduced to locate at the center of six sides of each hexagon (indicated by red dashed circles) because these columns exhibit apparently higher brightness (than Mg columns) that does not come from Nd atoms (in other words,

their higher brightness must come from Ag atoms). Viewed along the $[2\bar{1}\bar{1}0]_{\alpha}$ direction, Fig. 5b, brighter columns distribute in a shape of zig-zag chains. According to Nd map in Fig. 5e, the columns at each vertex of these zig-zag chains exhibit the enrichment of Nd, as indicated by yellow dashed circles in Figs. 5b and 5e. And again, higher brightness of other columns in such zig-zag chains (indicated by green dashed circles) are deduced to come from Ag atoms. Hence, Nd-containing and Ag-containing layers distribute alternately along the vertical direction, i.e. $[0001]_{\alpha}$. In Nd-containing layers, apart from the columns at the vertexes of the zig-zag chains (yellow dashed circles in Fig. 5b), their adjacent columns, like those indicated by yellow arrows, also exhibit the presence of Nd signal. But Nd signal is weak in a few of such columns, making it hard to find out the periodicity of Nd-rich columns. This might be caused by the overlapping of different domains along the viewing direction, which may reduce the packing densities of Nd atoms in such columns. Viewed along the $[01\bar{1}0]_{\alpha}$ direction, Nd-rich and Ag-rich columns can be clearly determined from Nd map and Ag map in Figs. 5f and 5i, which again illustrates that the Nd-containing and Ag-containing layers distribute alternately along the vertical direction, i.e. $[0001]_{\alpha}$.

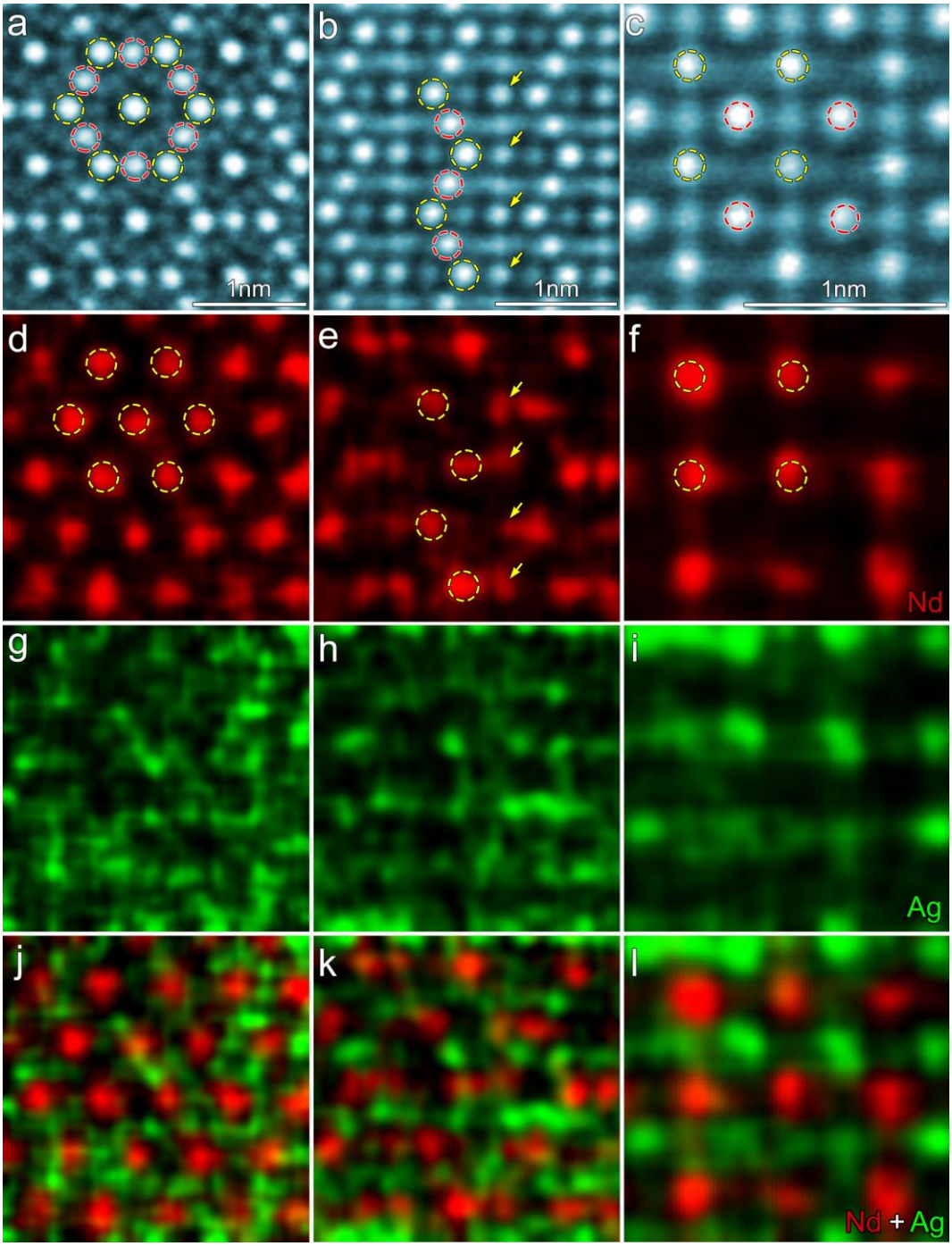

Fig. 5 (a-c) Atomic-resolution HAADF-STEM images of γ phase in a sample aged for 10 hours at 200 ºC. (d-l) Corresponding atomic-scale EDXS maps showing the distribution of Nd and Ag in HAADF-STEM images. Electron beam is parallel to $[0001]_{\alpha}$ in (a, d, g, j), $[2\bar{1}\bar{1}0]_{\alpha}$ in (b, e, h, k) and $[01\bar{1}0]_{\alpha}$ in (c, f, i, l).

According to the combined analyses of atomic-resolution HAADF-STEM images and EDXS maps, a possible atomic model of the γ phase is proposed, as shown in Fig. 6a. This model has a *P*6$_3$/*mmc* space group and 38 atoms in the unit cell (4 Nd atoms, 6 Ag atoms and 28 Mg atoms), and thus has a composition of $Nd_2Ag_3Mg_{14}$. Table 1 provides the atomic coordinates of the proposed model for γ phase. Based on this model, DFT calculations are applied to fully relax the structure. After relaxation, the output atomic model maintains its original symmetry (still of *P*6$_3$/*mmc* space group), and its cell volume, lattice parameters and atomic coordinates deviate only slightly from their

input values. The lattice parameters of the relaxed model are a = 1.00 nm, c = 0.99 nm, which are in good agreement with our experimentally measured lattice parameters, a = 0.99 nm, c = 1.03 nm. The formation energy of the structure is calculated to be -0.165 eV/atom, and the negative value indicates that the formation of γ phase is thermodynamically possible. Figs. 6b-6d show the projections along three principal zone axes of the relaxed model. Figs. 6e-6g provide the corresponding computer simulated HAADF-STEM images with experimental images inserted for comparation. The simulated images match well with the experimental images. The simulated image viewed along $[2\bar{1}\bar{1}0]_{\alpha}$ (Fig. 6f) exhibits a little difference with corresponding experimental image in those columns indicated by orange arrows, whose brightness is slightly lower in the experimental image than that in the simulated one. This might be caused by the overlapping of different domains along the viewing direction, which may reduce the packing densities of Nd in such columns. The current atomic model proposed for the γ phase is plausible under the experimental condition.

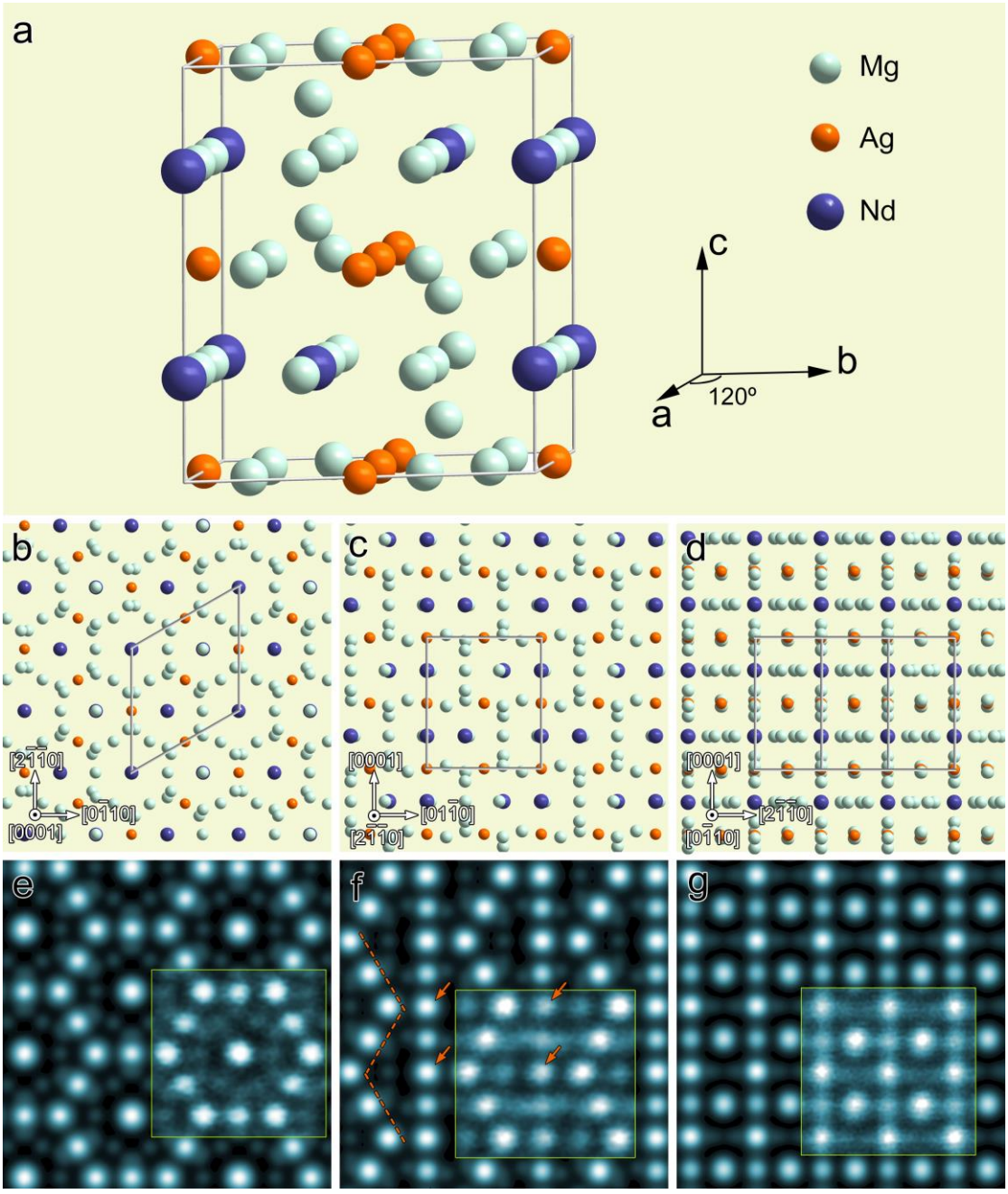

Fig. 6 (a) Atomic model proposed for γ phase. (b-d) Projections of the atomic model along $[0001]_{\gamma}$,

$[2\bar{1}\bar{1}0]_\gamma$ and $[01\bar{1}0]_\gamma$. (e-g) Corresponding simulated HAADF-STEM images of (b-d). Inserts in (e-g) are corresponding experimental HAADF-STEM images.

Table 1 Atomic coordinates of the proposed structure of γ phase

Atom	Wyck off site	*x*	*y*	*z*	Occupancy
Nd1	2b	0	0	0.250	1.00
Nd2	2d	0.667	0.333	0.250	1.00
Ag1	6g	0.500	0	0	1.00
Mg1	4f	0.667	0.333	0.600	1.00
Mg2	12k	0.333	0.167	0	1.00
Mg3	12j	0.333	0	0.75	1.00

3.2 Equilibrium δ precipitate phase

Investigation of the precipitates formed in samples aged at 150 ºC and 200 ºC illustrates that γ" and γ form successively during the ageing process. With further ageing, it is found that the γ phase and the equilibrium phase δ coexist inside individual particles. Even in samples aged for 420 hours at 250 ºC, the coexistence of γ and δ could still be observed (which is shown in section 3.3). Hence, to examine and establish the atomic structure of the δ precipitates, it is appropriate to firstly check the samples aged at even higher temperature, where only δ precipitate forms and the influence of γ" phase could be avoided. Fig. 7 shows the typical microstructure in a sample aged for 5 minutes at 300 ºC. Two types of precipitates can be clearly distinguished by in terms of particle size. In Figs. 7a and 7b, the smaller type of particles has a diamond shape with a size of around 12 nm, as indicated by the yellow arrows. This type of particles are proved to be the γ phase by atomic-resolution HAADF-STEM images (they are not shown to avoid repetition). The larger type of precipitates has an ellipsoid-shape, and is proved to be the equilibrium phase δ based on atomic-resolution images obtained. The δ particles have a typical size of about 30 nm when viewed along $[0001]_\alpha$ (as shown in Fig. 7b), and they have a tendency to elongate along the $[0001]_\alpha$ direction. The number density of the ellipsoid-shaped δ particle is much higher than that of the diamond-shaped γ particle at this ageing stage. EDXS maps provided in Figs. 7c-7f illustrate that both γ and δ contain Nd and Ag.

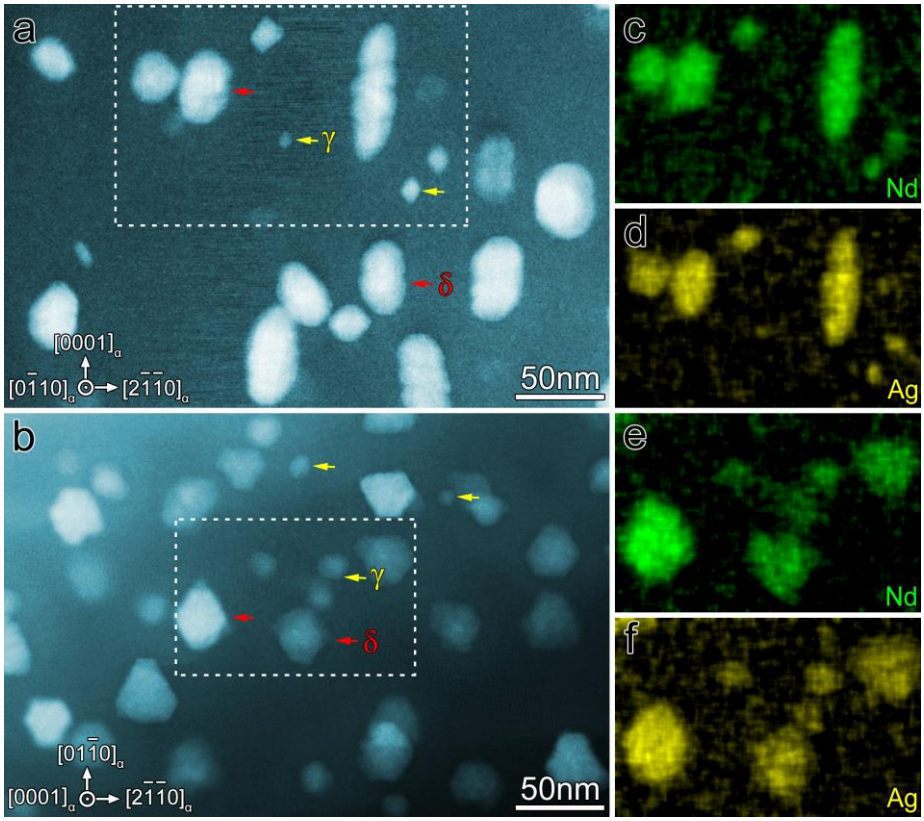

Fig. 7 (a, b) Low-magnification HAADF-STEM images showing precipitates γ and δ in a sample aged for 5 minutes at 300 ºC. (c, d) EDXS maps acquired in the dashed rectangle in (a). (e, f) EDXS maps obtained in the dashed rectangle in (b). Electron beam is parallel to $[0\bar{1}10]_\alpha$ in (a, c, d), and $[0001]_\alpha$ in (b, e, f).

When the ageing time is prolonged to about 15 minutes at 300 ºC, it is hard to detect the diamond-shaped γ particles. The atomic structure of the ellipsoid-shaped δ particles remains unchanged during ageing from 5 minutes to 4 hours, although most of δ particles have coarsened to be around 200 nm in samples aged for 4 hours at 300 ºC. Fig. 8 shows atomic-resolution HAADF-STEM images of the δ particles taken along three principal zone axes of the α-Mg matrix. Viewed along the $[2\bar{1}\bar{1}0]_\alpha$ direction, Fig. 8c, different domains with various atomic arrangements can be clearly observed within a single particle. However, when the viewing direction is parallel to $[0001]_\alpha$ or $[0\bar{1}10]_\alpha$, Fig. 8a or 8b, the entire region of the particle exhibits an identical atomic arrangement. This phenomenon can be invariably observed in individual δ particles and will be discussed in detail in section 4.1. Closer examination of the ellipsoid-shaped particles reveals that such particles are the equilibrium δ phase, because the atomic-resolution HAADF-STEM images taken along three directions in Figs. 8d-8f all exhibit similar atomic arrangements to those of the δ intermetallic phase (orthorhombic, a = 1.02 nm, b = 1.18 nm, c = 1.00 nm) [30]. The corresponding projections of the δ unit cell are provided at the bottom part of Fig. 8. The $[010]_\delta$ and $[001]_\delta$ projections of the δ unit cell match well with the corresponding images in Figs. 8e and 8f. However, in Fig. 8d, Ag-containing columns, which exhibit intermediate contrast, distribute irregularly in the columns located in the middle of two adjacent brightest columns, showing a little difference with the atomic model. This might be caused by the overlapping of different variants of δ phase along the viewing direction. The orientation relationship between δ phase and α-Mg matrix, obtained from Figs. 8a-8c, is such that $(100)_\delta$ // $(0001)_\alpha$ and $[001]_\delta$ // $[2\bar{1}\bar{1}0]_\alpha$.

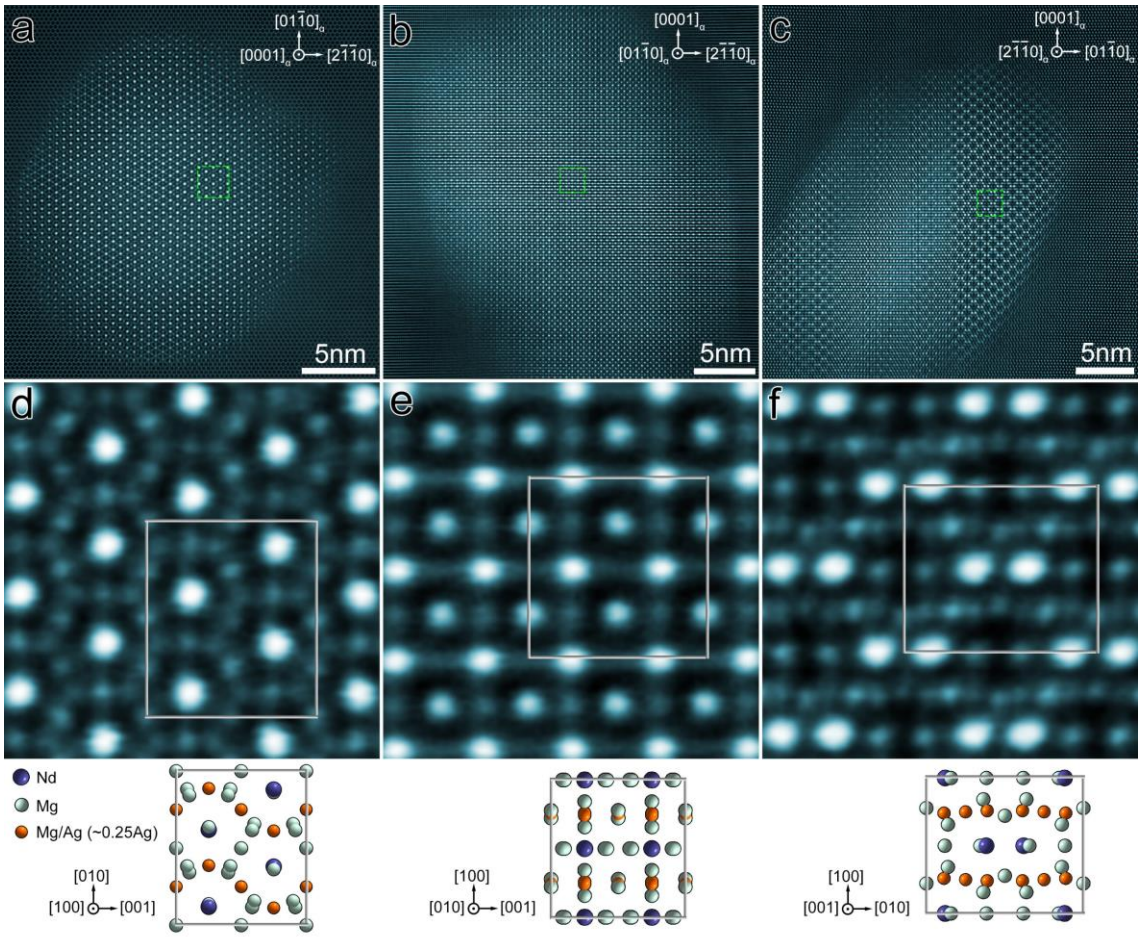

Fig. 8 (a-c) Atomic-resolution HAADF-STEM images showing the δ precipitates in a sample aged for 4 hours at 300 ºC. (d-f) Magnified views of the regions delimited with green dashed rectangles in (a-c), respectively. $[100]_\delta$, $[010]_\delta$ and $[001]_\delta$ projections of the δ atomic model are provided at the bottom of (d-e), respectively. Electron beam is parallel to $[0001]_\alpha$ in (a, d), $[01\bar{1}0]_\alpha$ in (b, e) and $[2\bar{1}\bar{1}0]_\alpha$ in (c, f).

3.3 Coexistence of γ and δ in individual particles

It is found in the present study that the coexistence of γ and δ inside individual particles could be invariably observed within a wide range of ageing time (24 to 420 hours) during ageing at 250 ºC. Fig. 9 shows the precipitates in a sample aged for 24 hours at 250 ºC. According to the low-magnification images shown in Figs. 9a and 9d, the precipitates have an ellipsoid shape with a size of about 30 nm (measured from the image in Fig. 9a) and tend to elongate along the $[0001]_\alpha$ direction (Fig. 9d). Fig. 9b shows the atomic arrangement of a particle viewed along $[0001]_\alpha$. The particle exhibits different domains with different atomic arrangements. In some domains, the bright columns are arranged in a shape of interconnected hexagons, which is the characteristic of the γ phase. These domains are thus regarded as γ phase. In other domains, the bright columns distribute in a shape of equilateral triangles, and some columns with intermediate contrast locate in the center of two adjacent brightest columns, as shown in the enlarged image in Fig. 9c. These domains have an atomic arrangement similar to that of the δ phase viewed along the $[100]_\delta$ direction, and thus they are treated as the δ phase. The width of the δ region varies, as indicated between two zig-zag dashed lines in Fig. 9c (the δ region). With an increase of the width, such regions become more readily to be recognized as the δ phase. The coexistence of the γ and δ phases inside a single particle is further confirmed when

viewed along the $[2\bar{1}\bar{1}0]_\alpha$ direction, as shown in Figs. 9e and 9f. The region with the characteristic of zig-zag chains is the γ phase, while the region at the top-right corner of the particle exhibits a similar atomic arrangement to that of the δ phase viewed along the $[001]_\delta$ direction. It concludes that the γ phase and the δ phase coexist inside individual particles at this ageing stage. In addition to the γ and the δ domains, the other regions in Figs. 9e and 9f exhibit complex atomic arrangements, which might be the result of overlapping of the γ and δ phases.

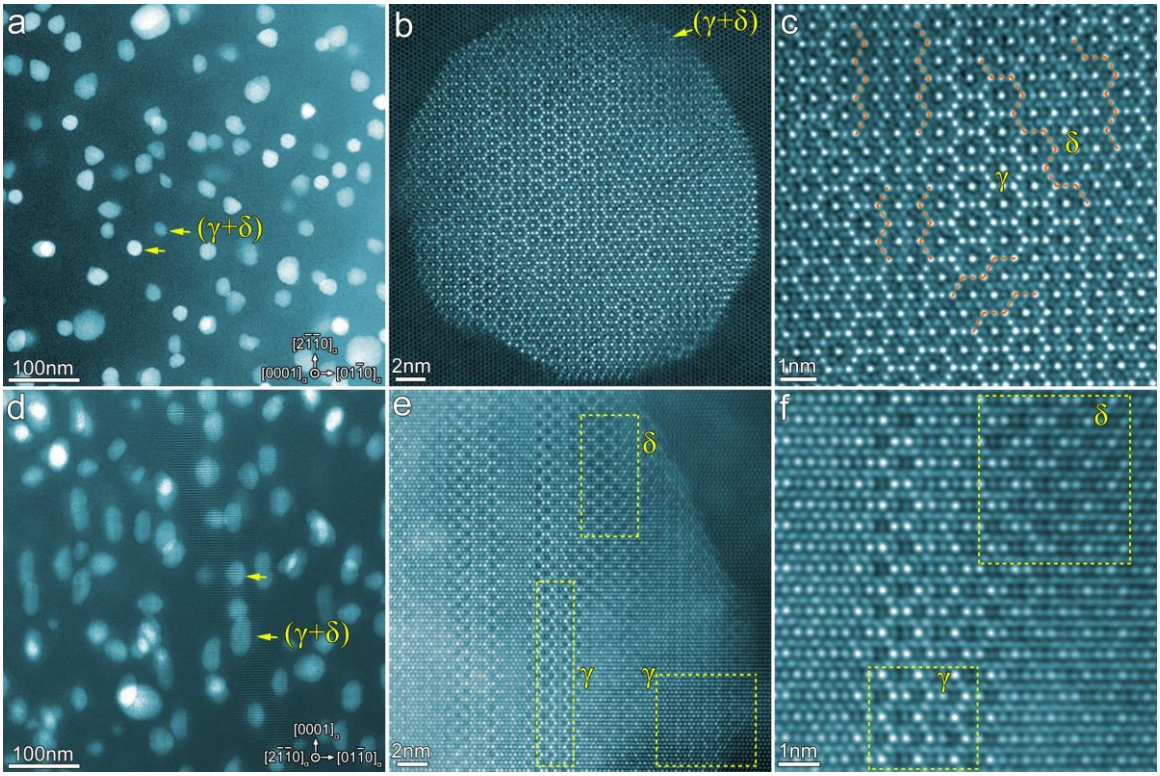

Fig. 9 HAADF-STEM images showing the coexistence of γ and δ phase in individual particles in a sample aged for 24 hours at 250 ºC. Electron beam is parallel to $[0001]_\alpha$ in (a-c) and $[2\bar{1}\bar{1}0]_\alpha$ in (d-f).

The coexistence of the γ and δ phases inside individual particles is quite stable when ageing is carried out at 250 ºC. Fig. 10a shows the precipitates formed in a sample aged for 420 hours at 250 ºC. Although most of the particles have coarsened to about 100-200 nm, the coexistence of the γ and δ phases inside individual particles could still be invariably observed. Fig. 10b provides a representative atomic arrangement of the particle, which clearly shows the γ and δ domains. At this ageing stage, a single particle contains a sufficient amount of δ domains so that they can be detected in a FFT pattern. Fig. 10c shows the FFT pattern acquired from Fig. 10b. The FFT pattern could be indexed by the combination of α-Mg, γ and three variants of δ, as illustrated in the schematic diagram in Fig. 10i, which is deduced from the schematic diagrams in Figs. 10d-10h. Hence, this information proves that a single particle at such ageing stage actually contains γ phase and three different variants of δ phase. Specifically, Figs. 10d-10f also provide FFT patterns for each δ variant, which are generated from corresponding regions indicated by yellow dashed squares in Fig. 10b. The crystals of distinct δ variants exhibit a 120° rotation with one another, and the $[002]_\delta$ direction of each δ variant is parallel to a specific $<11\bar{2}0>_\alpha$ direction. Therefore, δ phases form within the regions between γ domains with three different variants.

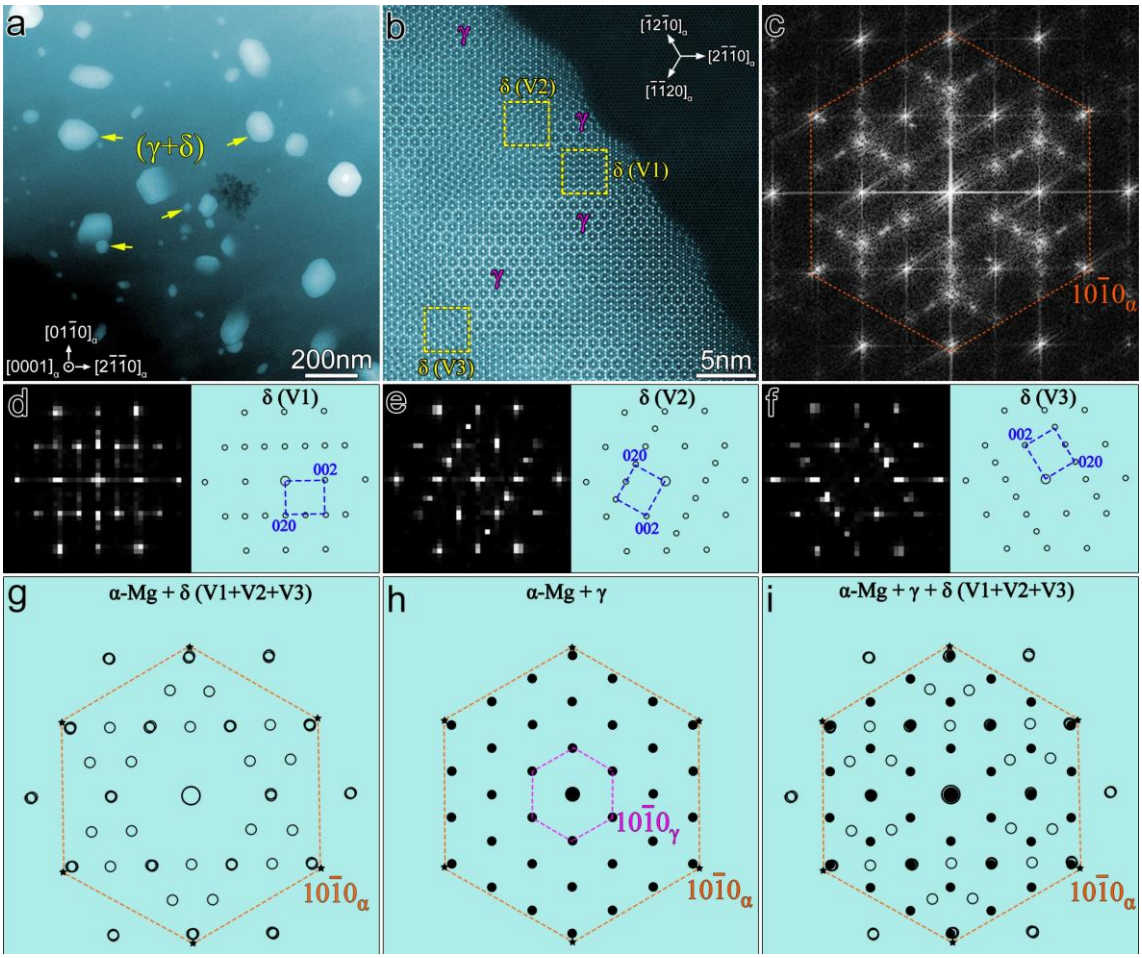

Fig. 10 (a) Low-magnification HAADF-STEM image showing the precipitates in a sample aged for 420 hours at 250 ºC. (b) Atomic-resolution HAADF-STEM image showing the coexistence of γ and δ phase in a single particle. (c) FFT pattern acquired from (b). FFT patterns in (d-f) are generated from yellow dashed squares in (b) labeled as δ (V1), δ (V1) and δ (V3), respectively. The schematic diagrams in (d-f) shows the ideal FFT patterns for three variants of the δ phase, i.e. V1, V2 and V3. The schematic diagrams in (g-i) illustrate the ideal FFT patterns resulting from the combination of multiple phases or variants, as indicated by the respective markings in each image. The schematic diagram in (i) agrees well with the actual FFT pattern in (b).

4. Discussion

4.1. Structure of the precipitate phases

It has been reported that the precipitation process of the QE22 alloy involves the formation of two metastable phases [27, 28]. The first one was determined by SAED to be the hexagonal χ phase (a = 0.286 nm, c = 0.521 nm) in a relatively recent work [28]. The χ phase, which was described as fine elongated precipitates, actually exhibits a similar morphology to the γ" phase observed in the present study. Based on atomic-scale characterization, the present work demonstrates that the first metastable phase is the hexagonal γ" phase (a = 0.56 nm, c = 0.45 nm), which has been widely observed at atomic scale in Mg-RE-Zn and Mg-RE-Ag alloys such as Mg-Gd-Zn, Mg-Nd-Zn, Mg-Sm-Zn, Mg-Y-Zn-Ag and Mg-Gd-Ag alloys [19, 21, 36, 37]. The orientation relationship between γ" and α-Mg is such that $(0001)_{\gamma''}$ // $(0001)_{\alpha}$ and $[01\bar{1}0]_{\gamma''}$ // $[2\bar{1}\bar{1}0]_{\alpha}$. A common feature of the γ" phase is that it forms as extremely thin plates on the $(0001)_{\alpha}$ basal plane with a thickness equivalent to only

one unit-cell (~0.45 nm, which varies slightly with alloying elements), which is associated with the large misfit along the habit plane normal of the γ" plates. Since the thickness of the γ" phase corresponds to two $(0002)_\alpha$ layers of α-Mg (0.521 nm), the misfit is approximately -0.136. The atomic-resolution HAADF-STEM images of the γ" phase observed along different zone axes in the present study of QE22 alloy are consistent with the proposed atomic model in the literature, which has been well studied by both experiments and DFT simulations in other Mg-RE-Zn and Mg-RE-Ag alloys [19, 37].

The second metastable phase reported in the literature is the hexagonal γ phase (a = 0.963 nm, c = 1.035 nm) [28]. The γ phase determined in the present work has a hexagonal structure (space group $P6_3/mmc$, a = 0.99 nm, c = 1.03 nm), similar to that reported in a previous work [28], and its orientation relationship with respect to the α-Mg matrix is such that $(0001)_\gamma$ // $(0001)_\alpha$ and $[2\bar{1}\bar{1}0]_\gamma$ // $[2\bar{1}\bar{1}0]_\alpha$. Its atomic model is proposed and validated in this study by atomic-resolution HAADF-STEM images, EDXS maps, DFT calculation and image simulation.

Interestingly, different domains are always found inside individual γ particles, even though the size of γ particle is only about 10 nm. Figs. 11a and 11b show the domain boundary (marked by white dashed lines) viewed along the $[0001]_\alpha$ and $[2\bar{1}\bar{1}0]_\alpha$ directions. The domain boundary appears to form by displacing one domain relative to the other along a vector (its two projections are indicated by the yellow arrows in Figs. 11a and 11b). Therefore, the domain boundary in the γ phase is characterized by a separation vector, analogous to the investigation of domain boundaries in a $Mg_{21}Zn_{25}$ intermetallic compound [38]. Based on the experimentally observed separation vectors indicated by the yellow arrows, a 3D atomic model of the γ lattice with a domain boundary embedded is generated, and its projections along $[0001]_\gamma$, $[2\bar{1}\bar{1}0]_\gamma$ and $[01\bar{1}0]_\gamma$ are provided in Figs. 11c, 11d and 11f, respectively. According to projections of the γ unit cell (white dashed frames) in Figs. 11c and 11d, it can be inferred that the separation vectors are $1/3[01\bar{1}0]_\gamma$ in Fig. 11c and $1/3[01\bar{1}0]_\gamma+1/2[0001]_\gamma$ in Fig. 11d. Hence, in 3D space, the separation vector related to the domain boundary is $1/3[01\bar{1}0]_\gamma+1/2[0001]_\gamma$. Given that the a_γ approximates to $3a_\alpha$, and c_γ approximates to $2c_\alpha$, the separation vector can be further written as $[1\bar{1}00]_\alpha + [0001]_\alpha = [1\bar{1}01]_\alpha$, under the observed orientation relationship between γ and α-Mg. Therefore, the separation vector associated with the domain boundary can be simply determined to be $[1\bar{1}01]_\alpha$. According to the $[01\bar{1}0]_\gamma$ projection of the atomic model of the γ phase with a domain boundary (Fig.11f), the domain boundary is invisible when viewed along this direction. The reason is that displacing one domain relative to the other along the separation vector would not cause apparent changes in arrangement of heavy atoms when viewed along the $[01\bar{1}0]_\gamma$ direction. This is consistent with the experimental observation that domain boundaries are invisible when viewed along the $[01\bar{1}0]_\alpha$ direction, like the example shown in Fig. 11e.

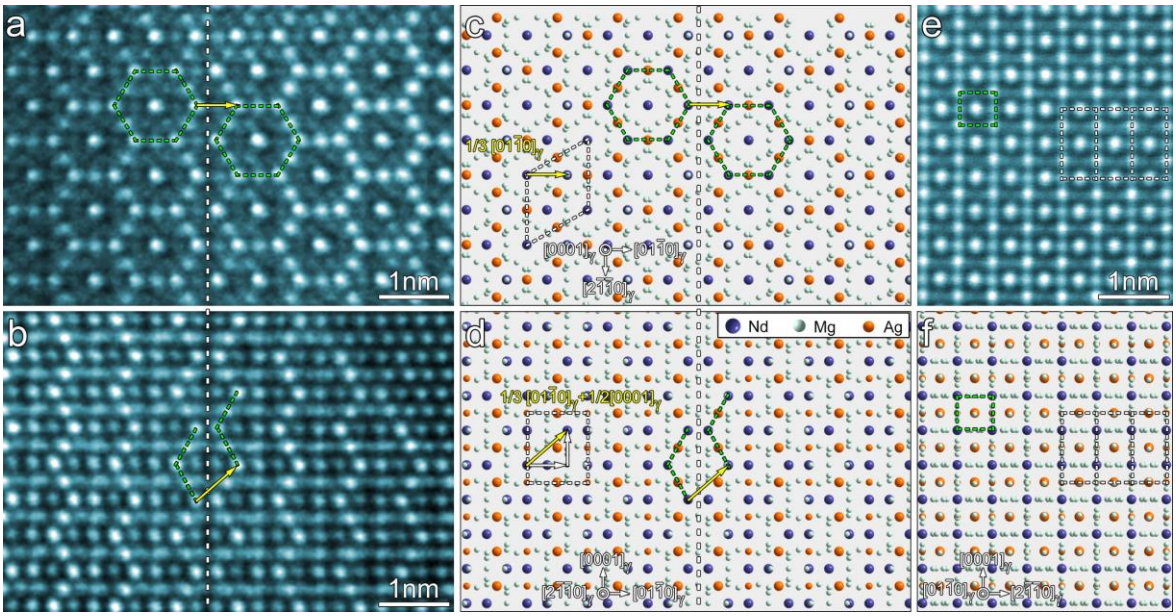

Fig. 11 (a, b) HAADF-STEM images showing the domain boundaries (white dashed lines) in γ phase. Electron beam is parallel to $[0001]_\gamma$ in (a) and $[2\bar{1}\bar{1}0]_\gamma$ in (b). The hexagons in (a) and the zigzag lines in (b) show the arrangement features of the bright dots in each image. The yellow arrows in (a, b) indicate the separation vectors of the arrangement features of each image. Following the separation vectors, a 3D atomic model of γ lattice with a domain boundary embedded is generated, and its projections along $[0001]_\gamma$, $[2\bar{1}\bar{1}0]_\gamma$ and $[01\bar{1}0]_\gamma$ are shown in (c, d, f), respectively. The white dashed frames in (c, d, f) indicate the projection of a γ unit cell. It can be inferred that the separation vectors indicated by the yellow arrows in (c, d) are $1/3[01\bar{1}0]_\gamma$ and $1/3[01\bar{1}0]_\gamma+1/2[0001]_\gamma$, respectively. (e) HAADF-STEM image showing the γ phase viewed along $[01\bar{1}0]_\alpha$ direction.

The present work demonstrates that the equilibrium precipitate phase is the δ phase (orthorhombic, a = 1.02 nm, b = 1.18 nm, c = 1.00 nm). The crystal structure of the δ phase has been well investigated in our previous work [30], where the δ phase is in the form of micron-sized intermetallic phase mainly distributed in grain boundaries. Compared to the δ intermetallic phase, the major difference of the δ precipitate phase formed inside the grain is that it contains different domains inside a single precipitate. Such domains are most likely to represent different variants of δ phase. According to the atomic-resolution HAADF-STEM images in Fig. 8, the δ precipitate adopts an exact orientation relationship with α-Mg, i.e., $(100)_\delta$ // $(0001)_\alpha$ and $[001]_\delta$ // $[2\bar{1}\bar{1}0]_\alpha$, which is shown in the stereographic projection in Fig. 12. According to the stereographic projection, when the viewing direction is $<2\bar{1}\bar{1}0>_\alpha$, images of the δ phase along $<001>_\delta$ or $<032>_\delta$ might be observed. And if the viewing direction is $<0\bar{1}10>_\alpha$, images of the δ phase along $<010>_\delta$ or $<012>_\delta$ might be observed. The atomic models of projections of the δ phase along different zone axes are provided in Fig. 13. The $[010]_\delta$ and $[012]_\delta$ projections shown in Figs. 13a and 13b are so similar that they cannot be distinguished by the atomic arrangement, which is the reason why different variants cannot be apparently recognized along the $[01\bar{1}0]_\alpha$ direction, as shown in Fig. 8b. The $[001]_\delta$ and $[032]_\delta$ projections in Figs. 13c and 13d are quite different. The arrangement of Nd-rich columns, which are expected to be the brightest columns in HAADF-STEM images, are totally different in these two projections, as indicated by the blue dashed circles in Figs. 13c and 13d. Different variants thus can be readily recognized along $[2\bar{1}\bar{1}0]_\alpha$, as shown in Fig. 8c. Hence, if different domains inside a single δ precipitate are accepted as different variants of δ phase, it can be explained why different domains can be found when viewed along $[2\bar{1}\bar{1}0]_\alpha$ rather than $[01\bar{1}0]_\alpha$.

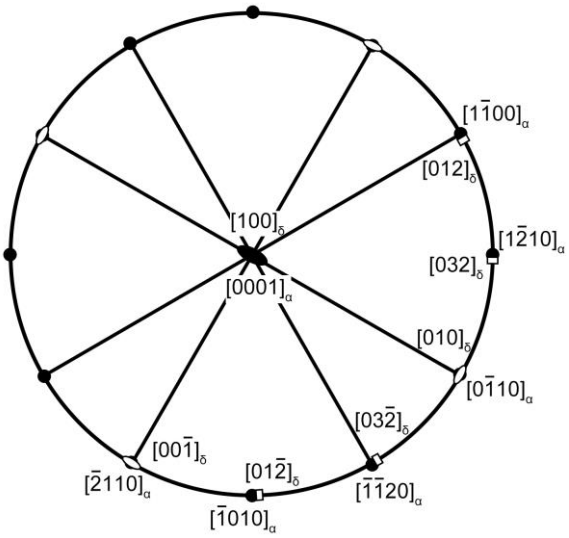

Fig. 12 Stereographic projection showing orientation relationship between δ phase and α-Mg matrix.

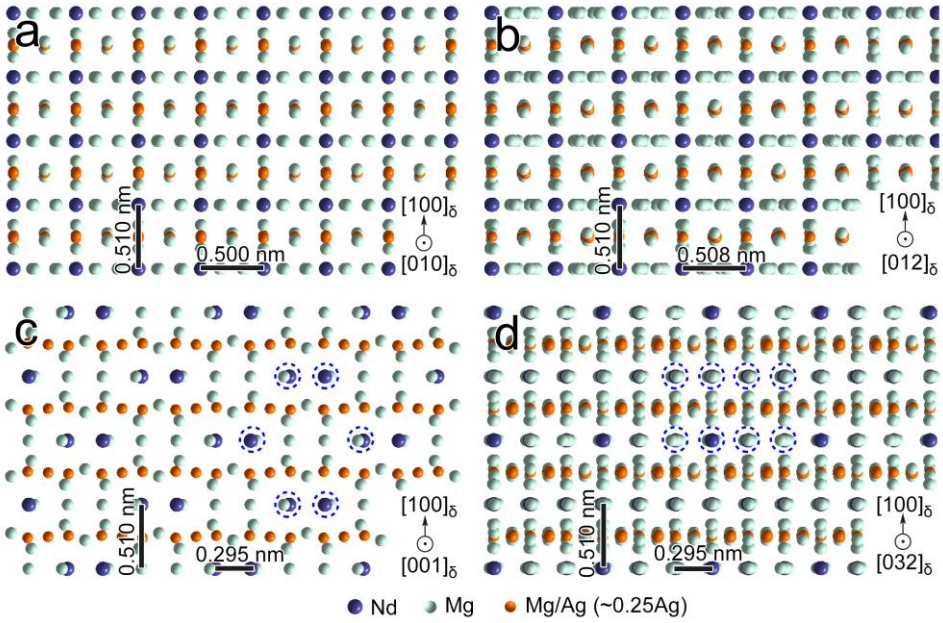

Fig. 13 Schematic diagrams showing projections of δ phase along (a) $[010]_\delta$, (b) $[012]_\delta$, (c) $[001]_\delta$ and (d) $[032]_\delta$. Blue dashed circles in (c) and (d) indicate Nd-containing columns.

To confirm the coexistence of different variants inside a single δ precipitate, enlarged images are provided in Fig. 14. Fig. 14a shows two variants of the δ phase viewed along $[2\bar{1}\bar{1}0]_\alpha$. In terms of the brightest columns, the atomic arrangement in region c is identical to that of the $[001]_\delta$ projection (Fig. 13c), while the atomic arrangement in region d is similar to that of the $[032]_\delta$ projection (Fig. 13d). The corresponding FFT patterns provided in Figs. 14c and 14d can be also indexed according to $[001]_\delta$ and $[032]_\delta$ zone axes of the δ phase, which is consistent with the analysis of the stereographic projection in Fig. 12. When viewed along $[0001]_\alpha$, Fig. 14b, different variants cannot be clearly distinguished by atomic arrangement, because the brightest columns distribute in a shape of equilateral triangle (Fig. 8), and the misorientation angle of the variants is 120°. The only feature that can distinguish the variants along the $[0001]_\alpha$ direction, is the regular distribution of Ag-rich columns,

as indicated by the atomic model in Fig. 8. However, as mentioned above, due to the overlap of different variants along the viewing direction, such regular distribution of Ag-rich columns can be recognized only in some short-range regions. Nevertheless, difference in FFT patterns of different regions is detectable, as shown in Figs. 14e-14g. The $[020]_\delta$ direction rotates 120º from one region to another, indicating that different regions of this particle contain different variants of the δ phase.

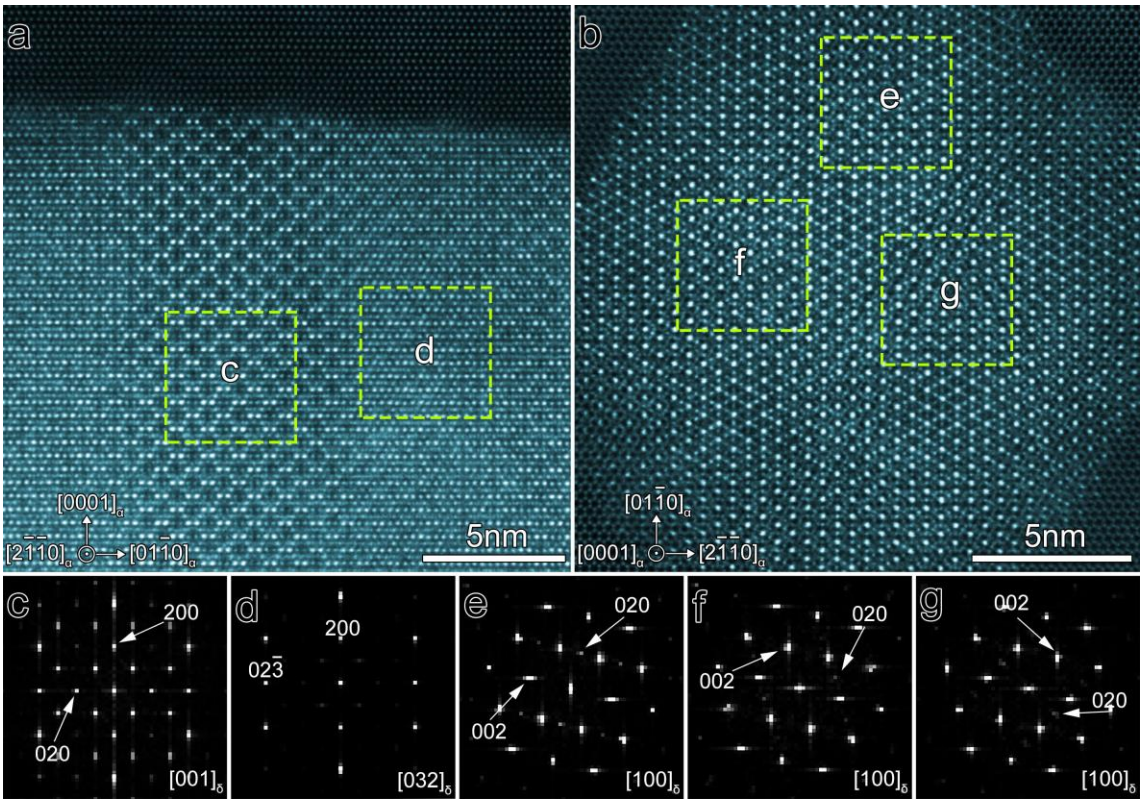

Fig. 14 (a, b) Atomic-resolution HAADF-STEM images showing the presence of different variants within individual δ precipitates in a sample aged for 4 hours at 300 ºC. (c-d) FFT patterns of regions c and d in (a). (e-g) FFT patterns of regions e, f and g in (b). Electron beam is parallel to (a) $[2\bar{1}\bar{1}0]_\alpha$ and (b) $[0001]_\alpha$.

4.2. Phase transformation between precipitate phases

As for the transformation from γ'' to γ, it has been observed that they are closely attached to each other in a sample aged for 1 hour at 200 ºC, indicating that the γ phase may nucleate at its precursor γ'' phase, as shown in Fig. 15. Viewed along the $[0001]_\alpha$ direction in Fig. 15a, the bright columns on the left are arranged in an equilateral triangle shape (characteristic of γ'' phase), while a hexagonal shape (characteristic of γ phase) begins to form on the right, as indicated by the dashed hexagon. Viewed along the $[2\bar{1}\bar{1}0]_\alpha$ direction in Fig. 15b, the arrangement of bright columns on the right are similar to that of the γ phase, which appears to nucleate at the thin γ'' basal plate.

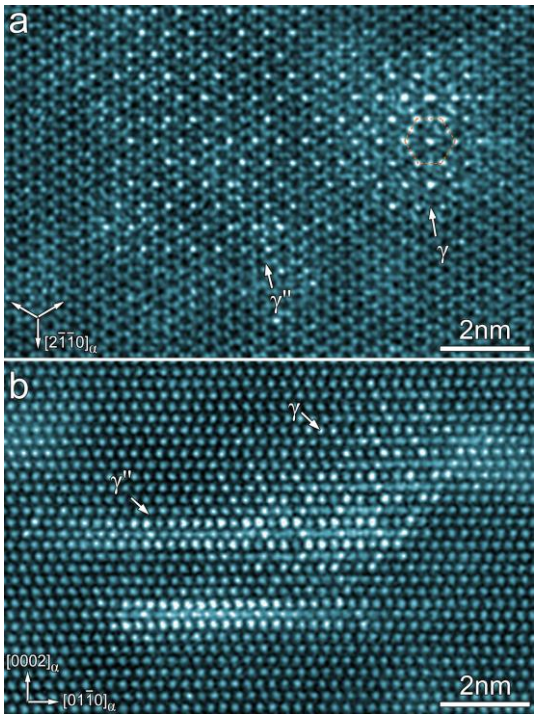

Fig. 15 HAADF-STEM images showing the attachment of γ'' and γ phases in a sample aged for 1 hour at 200 ºC. Electron beams are parallel to (a) $[0001]_\alpha$ and (b) $[2\bar{1}\bar{1}0]_\alpha$.

The presence of different variants inside a single δ precipitate suggests that the equilibrium δ phase forms *in situ* from its precursor metastable phase, like the β phase forms *in situ* from the β_1 phase in WE54 alloy [11]. On the other hand, the challenge of finding pure δ particles with a relatively small size (e.g., several nanometers) at all ageing states in the present study indicates the difficulty of direct nucleation of the δ phase in the α-Mg matrix. The coexistence of δ and γ phases inside individual particles suggests that the δ precipitate forms by *in situ* transformation from the γ phase. The γ particles observed at early ageing stage always contain domain boundaries (Fig. 4a). With further ageing, it seems that the domain boundaries gradually widen, and the δ phase emerges within the expanded regions between the γ domains (Fig. 9c and Fig. 10b). Therefore, it is highly likely that the δ phase first nucleates at the domain boundaries of the γ phase and then grows gradually at the expense of the γ phase. The domain boundaries inside the γ phase extend along three $<2\bar{1}\bar{1}0>_\alpha$ directions when viewing along $[0001]_\alpha$ direction (Fig. 4a). By analyzing the locations of different δ variants in Fig. 10b and Figs. 10d-10f, it is found that the $[002]_\delta$ of a certain δ variant tends to align parallel to the extending direction of the original domain boundary where the δ variant nucleates. For example, it is reasonable to assume that the original domain boundary where the δ (V1) nucleates extends horizontally in Fig. 10b (i.e. along the $[2\bar{1}\bar{1}0]_\alpha$ direction), and the $[002]_\delta$ of the δ (V1) is parallel to $[2\bar{1}\bar{1}0]_\alpha$. As a result, the three distinct extending directions of the domain boundaries of γ phase lead to three different δ variants.

Therefore, during the ageing process, the precursor γ'' phase may facilitate the nucleation of the γ phase, while the equilibrium δ phase directly forms *in situ* within the γ phase. All the transformation processes between two adjacent phases are most likely to be accomplished through diffusion of added alloying elements. Fig. 16 shows the comparison of atomic structures along three principal axes of α-Mg, γ'', γ and δ phases, indicating that they are similar in terms of atomic arrangement. For example, for γ'', γ and δ phases, Nd-containing columns are all arranged in an equilateral triangle shape when the view direction is $[0001]_\alpha$ // $[0001]_{\gamma''}$ // $[0001]_\gamma$ // $[100]_\delta$, as marked by the blue dashed circles in

Figs. 16d, 16g and 16j. Similar columns in terms of separation distance can be also picked up in the original α-Mg (marked by blue circles in Fig. 16a). Note that γ" only forms with one unit-cell thickness along the viewing direction due to the large misfit, the observation of γ" using HAADF-STEM imaging is strongly influenced by the Mg columns of the α-Mg matrix. The distribution of Nd-containing columns in γ" can be observed only in extremely thin areas of a TEM foil, while Ag-containing columns are still not observable (Fig. 3c and Fig. 15a). The possible reason for this is that Nd has larger atomic number than Ag. Due to the reason that Ag-containing columns are not observable in γ", the bright columns (only Nd-containing columns) form an equilateral triangle distribution. While in γ phase, Ag-containing columns are detectable, and they show almost the same brightness as Nd-containing columns because the number density of Ag is twice that of Nd along the viewing direction (see the numbers marked next to the blue or orange dashed circles in Fig. 16g). Hence, the bright columns (both Nd-containing and Ag-containing columns) now arrange in a regular hexagonal shape, as shown by the blue solid hexagonal frame in Fig. 16g. As for the δ phase, (Mg+Ag) sites contain only about 25% Ag, that is why Ag-containing columns are much darker than the Nd-containing columns. The bright columns (only Nd-containing columns) again arrange in an equilateral triangle shape. The similarity in atomic arrangement among α-Mg, γ", γ and δ phases is more pronounced when viewed along the other two principal directions, as emphasized by the blue rectangular frames in Fig. 16. The similarities in atomic structures of these precipitates may facilitate the phase transformations between them, as it requires a relatively small amount of diffusion of alloying elements to accomplish the transformations.

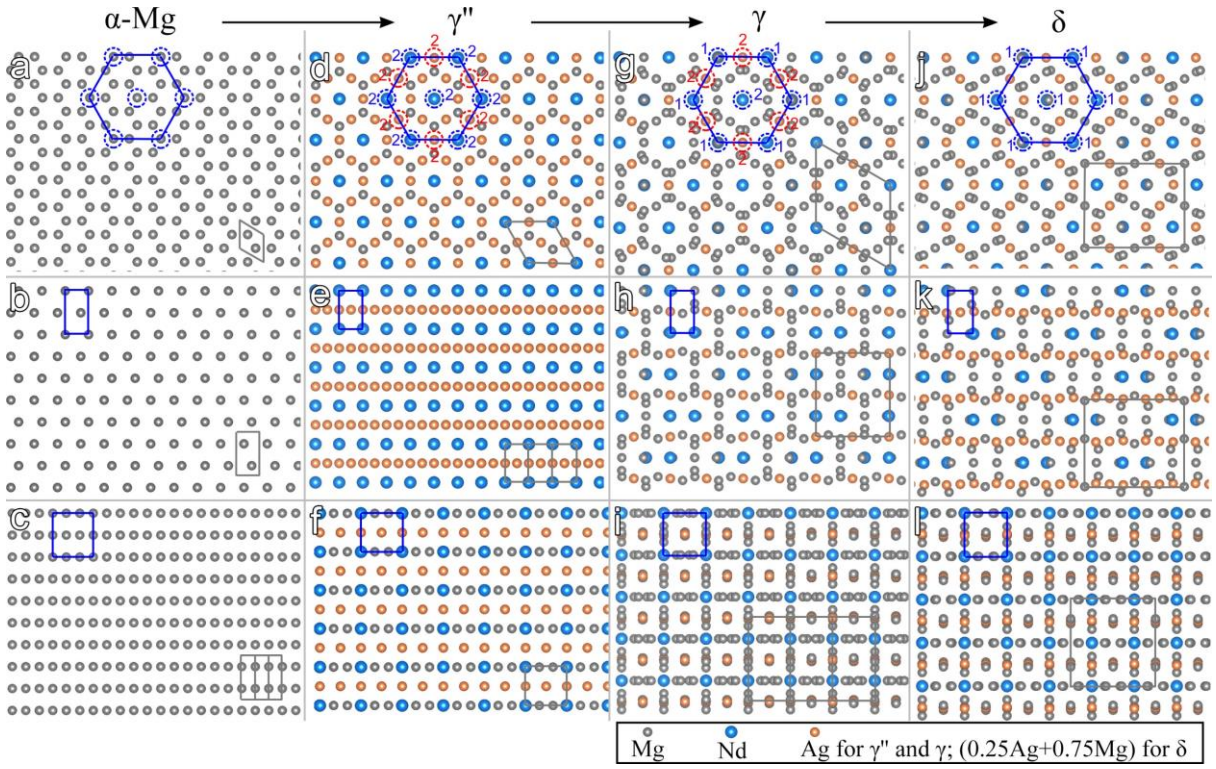

Fig. 16 Schematic diagrams showing the compassion of atomic structures of (a-c) α-Mg, (d-f) γ", (g-i) γ and (j-l) δ phases. According to the orientation relationships among them, the viewing directions are $[0001]_{\alpha}$ // $[0001]_{\gamma''}$ // $[0001]_{\gamma}$ // $[100]_{\delta}$ for (a, d, g, j), $[2\bar{1}\bar{1}0]_{\alpha}$ // $[01\bar{1}0]_{\gamma''}$ // $[2\bar{1}\bar{1}0]_{\gamma}$ // $[001]_{\delta}$ for (b, e, h, k) and $[01\bar{1}0]_{\alpha}$ // $[2\bar{1}\bar{1}0]_{\gamma''}$ // $[01\bar{1}0]_{\gamma}$ // $[010]_{\delta}$ for (c, f, i, l). The blue frames (sometimes together with blue or orange dashed circles) in each subgraph of every horizontal row are used to emphasize the similarity of the atomic arrangement. The numbers next to the dashed circles in (d, g, j) indicate

the number of heavy atoms Nd (blue circles) or Ag (orange circles) within a certain distance along the observation. This distance equals to (d) two γ" unit cells, (g) one γ unit cell and (j) one δ unit cell. Gray frames in each subgraph represent the projections of the corresponding unit cells.

5. Conclusions

Precipitate phases γ", γ and δ formed in QE22 alloy aged at 150-300 ºC have been comprehensively studied using atomic-scale HAADF-STEM imaging and atomic-scale EDXS mapping. The main conclusions are:

(1) The γ" phase forms as thin basal plates with a thickness of approximately 0.45 nm. The structure of the γ" phase is identical to γ" phases reported in Mg-Gd-Ag, Mg-Y-Zn-Ag, and Mg-Gd-Zn alloys, which has a hexagonal structure (a = 0.56 nm and c = 0.45 nm). The orientation relationship between γ" and α-Mg is such that $(0001)_{\gamma''}$ // $(0001)_{\alpha}$ and $[01\bar{1}0]_{\gamma''}$ // $[2\bar{1}\bar{1}0]_{\alpha}$.

(2) The γ phase forms as diamond-shaped particles and is the main strengthening phase in samples subjected to T6 treatment (200 ºC for 10 h). An atomic model is proposed for γ phase, and it has a hexagonal structure (space group $P6_3/mmc$, a = 1.00 nm, c = 0.99 nm) and a composition of $Nd_2Ag_3Mg_{14}$. The orientation relationship of γ phase and α-Mg is of the form $(0001)_{\gamma}$ // $(0001)_{\alpha}$ and $[2\bar{1}\bar{1}0]_{\gamma}$ // $[2\bar{1}\bar{1}0]_{\alpha}$. A single γ particle usually contains different domains, and the domain boundary can be characterized by a separation vector of $[1\bar{1}01]_{\alpha}$.

(3) The δ phase is the equilibrium phase that has an orthorhombic structure (space group *Cmcm*, a = 1.02 nm, b = 1.18 nm, c = 1.00 nm) and a composition of $NdAgMg_{11}$. The orientation relationship between δ and α-Mg is such that $(100)_{\delta}$ // $(0001)_{\alpha}$ and $[001]_{\delta}$ // $[2\bar{1}\bar{1}0]_{\alpha}$.

(4) The δ phase forms *in situ* from its precursor γ phase, leading to the formation of three different variants within a single δ particle. The nucleation of δ phase is strongly related to the domain boundaries of the γ phase. The *in-situ* transformation process is quite slow at 250 ºC, and the retained γ phase and three variants of δ phase can be observed inside individual particles even when the ageing time is prolonged to 420 hours. The nucleation of the γ phase may be promoted by its precursor γ" phase. The γ", γ and δ phases exhibit similarities in their atomic arrangements, which may facilitate the phase transformations between them through the diffusion of added alloying elements.

Acknowledgements

HWC acknowledges the support from the National Key Research and Development Program of China (2021YFB03702101), National Natural Science Foundation of China (52071033, 52101150), Sichuan Science and Technology Program (2022YFG0287), Fundamental Research Funds for the Central Universities (2682021CX114), and Project on Function Development of Large-scale Instruments of Chongqing University (gnkf2022017). JFN acknowledges the financial support from the Australian Research Council.

References

[1] B. Mordike, T. Ebert, Magnesium: properties—applications—potential, Mater. Sci. Eng. A 302 (2001) 37-45.
[2] J.F. Nie, Preface to viewpoint set on: phase transformations and deformation in magnesium alloys, Scripta Mater. 48 (2003) 981-984.
[3] T.M. Pollock, Weight loss with magnesium alloys, Science 328 (2010) 986-987.
[4] B.-C. Suh, M.-S. Shim, K.S. Shin, N.J. Kim, Current issues in magnesium sheet alloys: Where do we go from here?, Scripta Mater. 84–85 (2014) 1-6.
[5] I.J. Polmear, D. StJohn, J.F. Nie, M. Qian, Light alloys: Metallurgy of the light metals, fifth ed., Elsevier, London, 2017.
[6] Y.C. Zhou, Q. Luo, B. Jiang, Q. Li, F.S. Pan, Strength-ductility synergy in $Mg_{98.3}Y_{1.3}Ni_{0.4}$ alloy processed by high temperature homogenization and rolling, Scripta Mater. 208 (2022) 114345.
[7] C. Liu, X.H. Yang, J.C. Peng, B. Liu, Q. Luo, Q. Li, K.-C. Chou, In-situ and ex-situ investigation of deformation behaviors of a dual-phase Mg−Ni−Y alloy, Scripta Mater. 226 (2023) 115264.
[8] J.F. Nie, Precipitation and hardening in magnesium alloys, Metall. Mater. Trans. A 43 (2012) 3891-3939.
[9] Y.L. Guo, Q. Luo, B. Liu, Q. Li, Elastic properties of long-period stacking ordered phases in Mg–Zn–Y and Mg–Ni–Y alloys: A first-principles study, Scripta Mater. 178 (2020) 422-427.
[10] S. Zhang, Q.Q. Li, H.C. Chen, Q. Li, Icosahedral quasicrystal structure of the $Mg_{40}Zn_{55}Nd_5$ phase and its thermodynamic stability, Int. J. Min. Met. Mater. 29 (2022) 1543-1550.
[11] J.F. Nie, B.C. Muddle, Characterisation of strengthening precipitate phases in a Mg-Y-Nd alloy, Acta Mater. 48 (2000) 1691-1703.
[12] R. Wilson, C.J. Bettles, B.C. Muddle, J.F. Nie, Precipitation hardening in Mg-3wt%Nd(-Zn) casting alloys, Mater. Sci. Forum 419-422 (2003) 267-272.
[13] Q. Luo, Y.L. Guo, B. Liu, Y.J. Feng, J.Y. Zhang, Q. Li, K. Chou, Thermodynamics and kinetics of phase transformation in rare earth–magnesium alloys: A critical review, J. Mater. Sci. Technol. 44 (2020) 171-190.
[14] S.M. He, X.Q. Zeng, L.M. Peng, X. Gao, J.F. Nie, W.J. Ding, Precipitation in a Mg-10Gd-3Y-0.4Zr (wt.%) alloy during isothermal ageing at 250 degrees C, J. Alloys Compd. 421 (2006) 309-313.
[15] X. Gao, S.M. He, X.Q. Zeng, L.M. Peng, W.J. Ding, J.F. Nie, Microstructure evolution in a Mg-15Gd-0.5Zr (wt.%) alloy during isothermal aging at 250 °C, Mater. Sci. Eng. A 431 (2006) 322-327.
[16] Y. Zhang, W. Rong, Y.J. Wu, L.M. Peng, J.F. Nie, N. Birbilis, A detailed HAADF-STEM study of precipitate evolution in Mg–Gd alloy, J. Alloys Compd. 777 (2019) 531-543.
[17] Y.L. Guo, B. Liu, W. Xie, Q. Luo, Q. Li, Anti-phase boundary energy of β series precipitates in Mg-Y-Nd system, Scripta Mater. 193 (2021) 127-131.
[18] Y.M. Zhu, A.J. Morton, J.F. Nie, Improvement in the age-hardening response of Mg–Y–Zn alloys by Ag additions, Scripta Mater. 58 (2008) 525-528.
[19] Y.M. Zhu, K. Oh-ishi, N. Wilson, K. Hono, A.J. Morton, J.F. Nie, Precipitation in a Ag-containing Mg-Y-Zn Alloy, Metall. Mater. Trans. A 47 (2016) 927-940.
[20] Y. Zhang, W. Rong, Y.J. Wu, L.M. Peng, J.F. Nie, N. Birbilis, A comparative study of the role of Ag in microstructures and mechanical properties of Mg-Gd and Mg-Y alloys, Mater. Sci. Eng. A 731 (2018) 609-622.
[21] Y. Zhang, Y.M. Zhu, W. Rong, Y.J. Wu, L.M. Peng, J.F. Nie, N. Birbilis, On the precipitation in an Ag-containing Mg-Gd-Zr alloy, Metall. Mater. Trans. A 49 (2018) 673-694.
[22] Y. Zhang, T. Alam, B. Gwalani, W. Rong, R. Banerjee, L.M. Peng, J.F. Nie, N. Birbilis, On the role of Ag in enhanced age hardening kinetics of Mg–Gd-Ag-Zr alloys, Phil. Mag. Lett. 96 (2016)

212-219.
[23] Y. Zhang, Y.J. Wu, L.M. Peng, P.H. Fu, F. Huang, W.J. Ding, Microstructure evolution and mechanical properties of an ultra-high strength casting Mg–15.6Gd–1.8Ag–0.4Zr alloy, J. Alloys Compd. 615 (2014) 703-711.
[24] X. Gao, J.F. Nie, Enhanced precipitation-hardening in Mg–Gd alloys containing Ag and Zn, Scripta Mater. 58 (2008) 619-622.
[25] Q.D. Wang, J. Chen, Z. Zhao, S.M. He, Microstructure and super high strength of cast Mg-8.5Gd-2.3Y-1.8Ag-0.4Zr alloy, Mater. Sci. Eng. A 528 (2010) 323-328.
[26] R.J.M. Payne, N. Bailey, Improvement of the age-hardening properties of magnesium-rare-earth alloys by addition of silver, J. Inst. Met. 88 (1960) 417-427.
[27] K.J. Gradwell, Ph.D. Dissertation, University of Manchester, Manchester, 1972.
[28] G. Barucca, R. Ferragut, D. Lussana, P. Mengucci, F. Moia, G. Riontino, Phase transformations in QE22 Mg alloy, Acta Mater. 57 (2009) 4416-4425.
[29] J. Kiehn, B. Smola, P. Vostrý, I. Stulíková, K.U. Kainer, Microstructure changes in isochronally annealed alumina fibre reinforced Mg–Ag–Nd–Zr alloy, Phys. Stat. Soli. A 164 (1997) 709-723.
[30] X.J. Zhao, Z.Q. Li, H.W. Chen, R. Schmid-Fetzer, J.F. Nie, On the equilibrium intermetallic phase in Mg-Nd-Ag alloys, Metall. Mater. Trans. A 51 (2020) 1402–1415.
[31] G. Kresse, J. Furthmüller, Efficient iterative schemes for ab initio total-energy calculations using a plane-wave basis set, Phys. Rev. B 54 (1996) 11169-11186.
[32] J.P. Perdew, K. Burke, M. Ernzerhof, Generalized gradient approximation made simple, Phys. Rev. Lett. 77 (1996) 3865-3868.
[33] J.F. Nie, N.C. Wilson, Y.M. Zhu, Z. Xu, Solute clusters and GP zones in binary Mg–RE alloys, Acta Mater. 106 (2016) 260-271.
[34] L. Huber, I. Elfimov, J. Rottler, M. Militzer, Ab initio calculations of rare-earth diffusion in magnesium, Phys.Rev. B 85 (2012) 144301.
[35] A. Issa, J.E. Saal, C. Wolverton, Formation of high-strength beta' precipitates in Mg-RE alloys: The role of the Mg/beta" interfacial instability, Acta Mater. 83 (2015) 75-83.
[36] J.F. Nie, K. Oh-ishi, X. Gao, K. Hono, Solute segregation and precipitation in a creep-resistant Mg-Gd-Zn alloy, Acta Mater. 56 (2008) 6061-6076.
[37] X.F. Gu, T. Furuhara, T. Kiguchi, T.J. Konno, L. Chen, P. Yang, On the atomic structure of γ" phase in Mg-Zn-Gd alloy, Scripta Mater. 146 (2018) 64-67.
[38] L.F. Zhang, W.Z. Wang, W.W. Hu, Z.Q. Yang, H.Q. Ye, Nanometer-sized domain structure in complex $Mg_{21}Zn_{25}$ formed by eutectoid phase transformation in a Mg-Zn alloy, J. Alloys Compd. 745 (2018) 319-330.